Magnetic properties of MnF_2 and CoF_2 determined by implanted positive muons. I. Localization studies

R. De Renzi, G. Guidi, P. Podini, and R. Tedeschi
Department of Physics, University of Parma, I-43100 Parma, Italy

C. Bucci
Department of Physics, University of Parma, I-43100 Parma, Italy
and Experimental Physics Division, European Organization for Nuclear Research (CERN), CH-1211 Geneva 23, Switzerland

S. F. J. Cox
Rutherford Appleton Laboratory, Chilton, Oxfordshire OX11 0QX, United Kingdom
(Received 6 December 1983)

In order to define the characteristics of implanted positive muons as probes of the magnetic properties of materials, simple and well-known antiferromagnetic crystals have been studied: CoF_2 and MnF_2. The present paper aims to establish the localization of implanted muons in the temperature region of most interest, i.e., near the phase transitions and in the ordered phase. In the companion paper the measured magnetic features of the crystals are presented and compared with the available data from NMR, neutron scattering, and magnetic susceptibility measurements. The localization of muons has been inferred from the symmetry and magnitude of the frequency shifts and splittings of the muon-spin-rotation signal in the presence of external fields both above and below T_N. A unique site of localization is evident in CoF_2, which has octahedral symmetry, where the muon experiences a nearly pure dipolar field generated by the Co spins: the local field due to the spontaneous magnetization at low temperatures is 2280 G and corresponds to the value calculated from simple dipole sums. In MnF_2, some uncertainty still remains between the two octahedral- and tetrahedral-symmetry sites.

I. INTRODUCTION

Positive muons can be a valuable microscopic probe of the properties of magnetic materials. Muon-spin-rotation (μSR) spectra are similar in character to those expected of NMR—the frequencies indicating the local fields, and the linewidths the local spin dynamics—but μSR is virtually unique in providing this information from an interstitial site in the lattice. It is the purpose of this paper to demonstrate how the site occupied by the muon, as well as its dynamical state, may be systematically established. This is a prerequisite for a correct interpretation of the μSR data in regard to the magnetic properties of the host material. It is also of intrinsic interest, and relevant to a variety of physical and chemical phenomena, to establish this behavior for a particle which can be considered representative of a whole class of light interstitial impurities.

The present work constitutes an example of localization study in antiferromagnetic insulator systems. CoF_2 and MnF_2 were chosen as two representative members of a large family of difluorites. They are both very well characterized[1–4] and the rather complete knowledge of their magnetic behavior makes them well suited as a test case for μSR. The compansion paper (hereafter referred to as paper II) describes the properties that muons are able to detect, both those which confirm existing data—and which therefore validate the μSR technique—as well as those which are unique to μSR.

The structure of the two salts is tetragonal of the rutile type, and their transition-metal spins align themselves in antiferromagnetic order below the Néel temperature, which is 67.336 and 37.85 K for the manganese and the cobalt crystals, respectively. This order is characterized by the existence of two tetragonal sublattices of transition-metal cations combined to give the body-centered structure of the crystal. While MnF_2 has a very small anisotropy, CoF_2 displays a large anisotropy that makes it a standard case of the three-dimensional (3D) Ising model.

Early experiments on both crystals[5,6] have given evidence of a coherent localization of the muon at sites of well-defined symmetry at low temperatures. Furthermore, it was possible to determine that the muon was experiencing different contributions from the magnetization of the two sublattices. In order to ascertain the nature of the site—or sites—where the particles come to rest, various kinds of experiments are possible.

For the paramagnetic phase, the externally induced polarization of the transition-metal electronic magnetic moment is expected to produce a small local magnetic field at the muon site with a well-defined angular dependence, whose details are determined by the nature of the interaction. This is recognized as a shift of the measured precession frequency relative to the free Larmor frequency appropriate to the applied field. The existence of two sublattices must also determine, in the general case, splittings of the frequency of the lines for particular orientations of

the magnetic field.

Below the Néel point the ordering of the magnetic moments is expected to produce a net field at those sites that are inequivalently placed with respect to the two opposite sublattices. If muons localize in such sites, the measurement of the local field due to the spontaneous magnetization both in the absence and in the presence of an externally applied magnetic field yields further information on the symmetry of the site.

In Sec. II a description of the experimental apparatus is given together with a brief outline of the principles of the technique. Section III contains an account of the measurements performed on the CoF_2 crystal, where all the effects described above allowed the determination of the symmetry of the site. In order to identify it, a calculation of the electrostatic potential at various possible interstitial sites, within the approximation of a rigid lattice of point charges, is reported in Sec. IV. The local-field tensor is also evaluated for pointlike dipoles using the values for the susceptibility tensor obtained from the literature. Finally, in Sec. V the comparison between the experiments and the predictions of the model lead to a unique determination of the localization site for the μ^+ in CoF_2. The description of similar experiments performed on MnF_2 indicates the same symmetry. Further comments and conclusions are given in Sec. VI.

II. EXPERIMENTS

A. Technique

All the data presented in this paper derive from the particular version of μSR which is known as muon spin rotation. Positive muons are implanted in a sample where they come to rest at particular sites within the lattice. There they precess in whatever magnetic fields, transverse to their initial polarization they experience changes at these sites. This precession may be monitored by detecting the positrons from the radioactive decay of the muons in a telescope of counters that defines a specific direction. Owing to parity violation, these positrons carry information about the spin precession by means of an anisotropy in the angular distribution of their emission probability, which is peaked around the muon spin direction. The events are collected in a histogram, as a function of the individual muon's lifetime, which has the general form

$$N(t)=N_0\left[e^{-t/\tau_\mu}\left\{1+\alpha\sum_i A_i P_i(t)\cos(2\pi\nu_i t+\varphi)\right\}+B\right], \tag{1}$$

where $\tau_\mu=2.2$ μs is the average μ^+ lifetime, α the anisotropy factor (averaging over the energies of the emitted particles $\alpha=\frac{1}{3}$, but experimental effects typically reduce its value to 0.24), ν_i the frequency of the ith component in the precession, $P_i(t)$ its spin relaxation function, A_i its weight, φ an initial phase, and B a constant background fraction of random events. The time histogram can be Fourier transformed, after correction for the exponential decay and the background, to yield the frequencies and amplitudes. In addition, fitting procedures give a more accurate determination of all parameters. In the present work minimization routines based on the CERN MINUIT package were adopted.

B. Sample and the spectrometers

The experiments were performed on a CoF_2 single crystal purchased from Cristaltec, Grenoble, where it was grown by the Bridgman method. Its shape is that of a cylinder of 15 mm diameter by 35 mm height, plus the typical conical extremity from which the growth was started. The sample was cut into approximate halves perpendicularly to the cylinder axis in order to allow all orientations in the experimental geometry. The experiments were carried out at European Organization for Nuclear Research (CERN), making use of both the CJ2 and the LJ1 muon channels of the 600-MeV synchrocyclotron.[7]

For most measurements conventional scintillation spectrometers were used, both in the transverse geometry (positron detectors at $\pm 90°$ from the beam direction) and in the longitudinal geometry in zero applied magnetic field. A set of crucial experiments required the use of our new wire-chamber spectrometer[8] that allows the collection of histograms containing events from the sample only. This feature was essential in all those cases in which the signal from the muons stopped in the cryostat walls and in the sample holder would have interfered with the relevant signal from the sample itself. The apparatus achieves the separation of the two contributions by allowing the spatial reconstruction of each event with an overall resolution of 5 mm. The muon and positron tracks are evaluated with the coordinates supplied by pairs of wire chambers added to the conventional telescopes. Figure 1 shows a typical image of the CoF_2 crystal inside the cryostat, as obtained

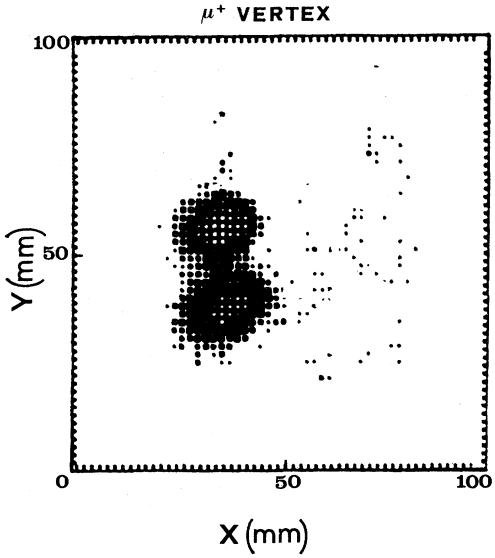

FIG. 1. Vertex reconstruction of the muon-decay events in the CoF_2 crystal performed with the wire-chamber spectrometer. The figure represents a cross section of the 3D histogram perpendicular to the muon beam. The image is slightly blurred because of the moment-dependent effect that the 3-kG magnetic field has on the position tracks.

by plotting all the detected μ-decay vertices; their comparison with the coordinates of the sample boundary would then constitute the criterion for acceptance of an event in the time histogram. Another characteristic of this new apparatus is that the detection is possible directly from the first few nanoseconds of life of the muons. As a consequence even very fast decaying signals ($\lambda < 10\ \mu s^{-1}$) could, in principle, be observed in the time histogram.

A helium flow and a closed-circuit helium cryostat were used; the temperature was stabilized by means of a commercial temperature controller unit driven by a resistance bridge, and the sensor was a platinum resistor. One of the two refrigerators allows the rotation of the sample: The resulting overall accuracy in sample alignment is of the order of $\pm 2°$. The crystal axis had been previously determined by x rays and by NMR measurements of the ^{19}F resonance splitting, with an accuracy of $\pm 1°$.

III. EXPERIMENTAL RESULTS

A. CoF_2

In the paramagnetic phase a signal was observed oscillating at the Larmor frequency. The muon fraction contributing to this signal was calibrated with a wire-chamber experiment, in which a reference copper sample of suitable thickness was contained inside the cryostat together with the CoF_2 crystal (the spatial resolution of events which is the feature of the wire-chamber spectrometer equally allows the simultaneous accumulation of μSR histograms from two or more samples in this way). By assuming no depolarization in copper, a comparison between the two simultaneous experiments determined that 70% of the implanted muons contribute to the observed precession in the cobalt salt.

Far above T_N this precession exhibits a decay rate of $0.5\ \mu s^{-1}$ (assuming Lorentzian relaxation), which remains fairly constant with temperature. The behavior of the decay rate close to T_N will be discussed in paper II.

By cooling the sample below T_N the Larmor frequency disappeared, and, when the crystal c axis was oriented perpendicular to the beam polarization, a temperature-dependent frequency was observed in the Fourier transform of longitudinal telescope histograms. The amplitude of this signal accounts for 44% of the detected muons. The total disappearance of the Larmor component was checked by means of the wire-chamber spectrometer: No signal was found at this frequency even at the beginning of the histograms.

B. Line shifts and splittings for $T > T_N$

When the external magnetic field is applied along the c axis the measurement performed with the wire-chamber spectrometer indicates a single frequency whose absolute paramagnetic shift was determined by use of a proton NMR probe. In the scintillator spectrometer the μ^+ precession in the crystal coexists, although slightly shifted, with the μ^+ precession in the cryostat walls. The isolated component due to the cryostat can be measured directly, in the same setup, at $T < T_N$. Two-wave fittings yield the paramagnetic shift relative to the Larmor frequency in the cryostat. The result, in both cases, is $\Delta B = -20$ G. The angular dependence of the shift was obtained by turning the a axis of the crystal toward the magnetic field: In this case, as it appears directly from the Fourier spectra, a splitting of the μ^+ precession in the crystal occurs, whose magnitude increases as the field direction approaches the a axis. The corresponding fitting is shown in Fig. 2. This splitting must be related to the tensorial character of both the susceptibility and the coupling between the muon and the polarized electron spins; its symmetry properties are very valuable in determining the site occupied by the muon, as will be discussed in Sec. IV.

Further experiments at 40 K, in which the external field was rotated within the $(\hat{a},\hat{b})$ plane of the crystal, showed as many as three resolvable components from the CoF_2 sample. In these cases, in order to reduce the number of variable parameters in the fit, all muon fractions stopped in the sample were bound to sharing the initial phase and the relaxation rate; their amplitudes were kept in fixed ratios.

In order to ascertain the nature of such multiplets of lines the wire-chamber spectrometer was used for a given crystal orientation. The magnetic field was oriented in this case in the $(\hat{a},\hat{b})$ plane at 22.5° from the a axis. Owing to the spatial resolution of the wire chambers, the μSR histogram did not contain any contribution from background muons. It was thus possible to obtain direct

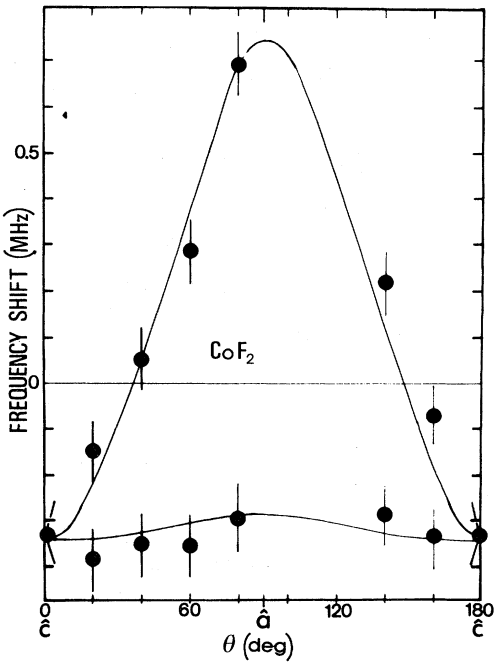

FIG. 2. Angular dependence of the frequency shift in CoF_2 at 41 K for a rotation of the crystal around the a axis. The external magnetic field then takes various orientations in the plane. Along the c axis no splitting is present while the maximum splitting is observed along the a axis. The "zero" shift for the continuous line (calculated from Sec. IV) has been arbitrarily corrected by 100 kHz (this correction could account for the small demagnetization effect).

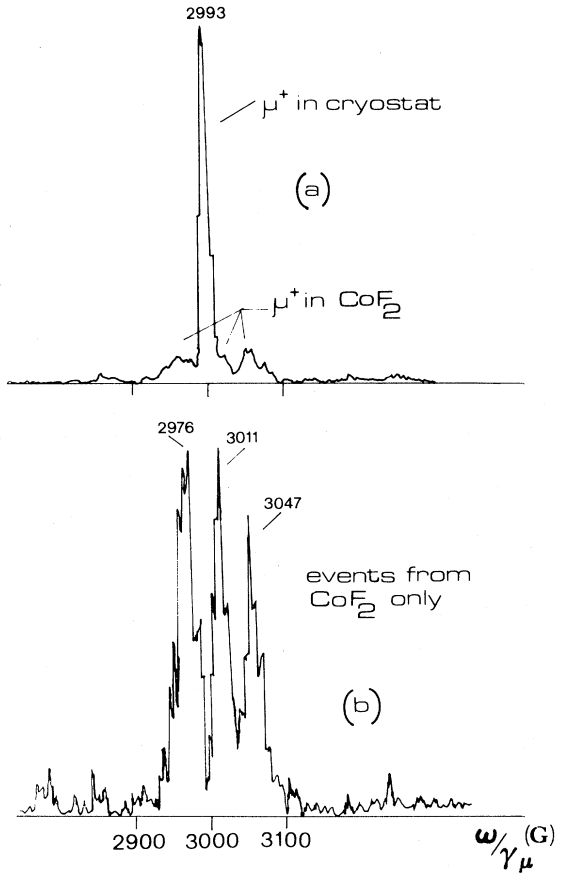

FIG. 3. Splittings of the precession frequencies in CoF_2 at 40 K in a field of 3 kG oriented in the $(\hat{a},\hat{b})$ plane at 22.5° from the b axis. Results from the conventional scintillator spectrometer in (a) are compared to those from the wire-chamber spectrometer in (b). The undesired signal from various materials surrounding the crystal in (a)—mainly the cryostat walls—is not present in (b) were signal analysis is correspondingly easier.

and convincing evidence of the three frequencies previously found in the rather critical fitting of the data from the scintillator spectrometer. The Fourier spectra relative to the two spectrometers can be compared in Fig. 3.

C. Hyperfine frequencies and field-induced splittings below T_N

The signal resulting from the spontaneous magnetization was studied in a wide range of temperatures below T_N. The extrapolation of the experimental data to $T=0$ gives a value of 2288 ± 1 G for the field generated by the spontaneous magnetization at the muon site $\vec{B}_{hf}$ (hf represents hyperfine). The details of the temperature dependence are given in paper II. The application of an external field at different orientations relative to the crystal axis confirmed the alignment of $\vec{B}_{hf}$ with the c axis, within the accuracy of our sample orientation. Upon applying an external field $\vec{B}_0$, the expected precession frequency will become

$$\nu_\mu=\frac{\gamma_\mu}{2\pi}\,|\vec{B}_0+\vec{B}^{\,i}_{hf}(T)\,| \qquad (2)$$

as demagnetization and Lorentz contributions are negligible. Here the index refers to the two crystal sublattices α and β, where the hyperfine fields have opposite signs ($\vec{B}^{\alpha}_{hf}=-\vec{B}^{\beta}_{hf}$). When $\vec{B}_0$ is exactly perpendicular to the c axis expression (2) predicts one single frequency, whereas the general case produces a doublet, as is shown in Fig. 4(a). Each of these frequencies should manifest a fine structure, however, characteristic of the symmetries of the localization sites, just as in the paramagnetic phase.

This fine structure was determined in a set of measurements at 13 K, with $\vec{B}_0$ nearly perpendicular to the c axis: a misalignment of 14° was purposely chosen in order to avoid the interference of the spectra belonging to the two sublattices. Rotations of the sample around this direction (near to the c axis) were performed by keeping the tilting angle constant to within ±1°. Figure 4(b) illustrates the results of these measurements and Fig. 4(c) shows a Fourier spectrum for one particular orientation. The pattern is consistent with that emerging from the experiments above T_N.

In all the measurements of an angular dependence in an external field no explicit correction has been made for the demagnetization field. The shape of the crystal does not

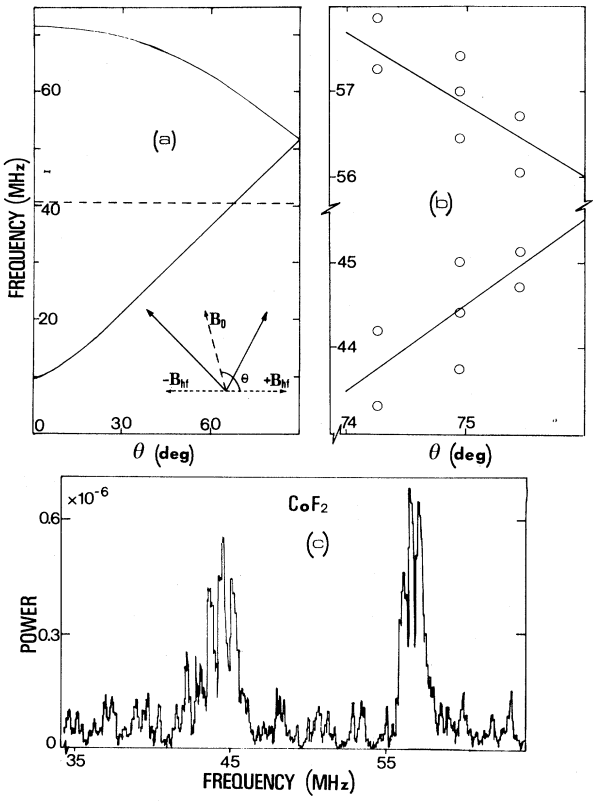

FIG. 4. (a) Muon frequencies for CoF_2 below T_N (13 K) in an external field (3 kG) reflect the vectorial composition of the applied field with that due to the spontaneous magnetization of each sublattice; (b) in addition each is split by the paramagnetic contribution induced by the applied field with the symmetries of the tensor $\vec{\vec{J}}$; when the external field is nearly perpendicular to the hyperfine field and at 22.5° from the b axis, each sublattice displays the same triplet (c) as for the paramagnetic phase (Fig. 3).

allow a simple evaluation of it, and it was empirically established, in any case, that the effects of the demagnetization reduce to a small constant correction to all frequencies and, possibly, a small contribution to the inhomogeneous broadening of the signals. Neither effect interferes with the analysis of the data in relation to the symmetry properties of the localization site of the muons.

IV. POSSIBLE SITES FOR THE MUON

A. Description of the crystal

In order to interpret the reported data we consider here the details of the crystalline and magnetic structure of CoF_2, and determine the possible sites of localization for the muon. Figure 5 shows the crystal unit cell: the translational symmetry is tetragonal. In the cell there are two F—Co—F molecular groups, which belong respectively to sublattices α and β: sublattice α has the metal cation in an inversion point with the two F^- at $(\pm\lambda,\pm\lambda,0)$, with $\lambda=0.31$; the other sublattice, β, is obtained by rotating α by $\pi/2$ around $\hat{c}$ and translating it by (0.5,0.5,0.5). Symmetry planes that contain the metal cation are perpendicular to $\hat{c}$, to $\hat{a}+\hat{b}$, and to $\hat{a}-\hat{b}$. Axes of binary symmetry parallel to $\hat{c}$ pass either through the metal cation or through the midpoint between two neighboring metal cations. Each metal cation is therefore surrounded by an octahedron of six F^- ions having rhombohedral distortion.

B. Local-field tensor

At temperatures below T_N spontaneous magnetization sets in along the c axis, the two sublattices having antiparallel ordering. Because of the crystal symmetry, the transverse susceptibility of the crystal as a whole is isotropic around the c axis; this does not hold true for the transverse susceptibility of each sublattice, $\chi_\perp^\alpha$ and $\chi_\perp^\beta$, whose principal axes are $\hat{a}+\hat{b}$ and $\hat{a}-\hat{b}$, respectively. A rotation by $\pi/2$ around $\hat{c}$ brings $\chi_\perp^\alpha$ into $\chi_\perp^\beta$.

A general expression for the magnetic field $\vec{B}_\mu^i(T)$ sensed by the muon at site i must include the externally applied field, the field due to the spontaneous magnetization (for $T<T_N$), $\vec{B}_{hf}(T)$, and the field due to the magnetization induced by the external field $\vec{B}_{ind}$:

$$\vec{B}_\mu^i(T)=\vec{B}_0+\vec{B}_{hf}^i(T)+\vec{B}_{ind}^i(T,\vec{B}_0)\ . \tag{3}$$

When $\vec{B}_0$ is well below saturation $\vec{B}_\mu(T)$ can be written in a more explicit form, without loss of generality, by defining the coupling tensor for each sublattice $\overleftrightarrow{D}_\alpha^i$ and $\overleftrightarrow{D}_\beta^i$ and the corresponding spontaneous magnetization per spin, $\mathcal{M}_{sp}(T)\hat{c}$:

$$\begin{aligned}\vec{B}_\mu^i(T)&=\vec{B}_0+(\overleftrightarrow{D}_\alpha^i-\overleftrightarrow{D}_\beta^i)\cdot\mathcal{M}_{sp}(T)\hat{c}\\&\quad+[\overleftrightarrow{D}_\alpha^i\cdot\overleftrightarrow{\chi}_\alpha(T)+\overleftrightarrow{D}_\beta^i\cdot\overleftrightarrow{\chi}_\beta(T)]\cdot\vec{B}_0\\&=\vec{B}_0+\vec{B}_{hf}^i(T)+\overleftrightarrow{J}^i(T)\cdot\vec{B}_0\ ,\end{aligned} \tag{4}$$

where $\overleftrightarrow{\chi}_j$ is the susceptibility per spin of sublattice j and the tensor $\overleftrightarrow{J}^i(T)$ is nonsymmetric, since $\overleftrightarrow{\chi}$ and $\overleftrightarrow{D}$ do not necessarily commute.

Since the μSR frequency at site i is determined by $|\vec{B}_\mu^i|$, we see that, for $T>T_N$ (where $\vec{B}_{hf}$ vanishes), after neglecting terms in $O(J^2)$,

$$|\vec{B}_\mu^i|^2=|\vec{B}_0|^2+2(\vec{B}_0\cdot\overleftrightarrow{J}^i\cdot\vec{B}_0)\ , \tag{5}$$

i.e., only the symmetric part of $\overleftrightarrow{J}^i$ contributes to the shift.

For $T<T_N$ the situation is slightly more complicated by the presence of $\vec{B}_{hf}^i(T)$:

$$\begin{aligned}|\vec{B}_\mu^i|^2&=|\vec{B}_0+\vec{B}_{hf}|^2+2(\vec{B}_0\cdot(\overleftrightarrow{J}^i\cdot\vec{B}_0)+[\vec{B}_0\cdot(\overleftrightarrow{J}^{iT}+\overleftrightarrow{J}^i)\cdot\vec{B}_{hf}^i]\\&\quad+[\vec{B}_0\cdot(\overleftrightarrow{J}^{iT}-\overleftrightarrow{J}^i)\cdot\vec{B}_{hf}^i]\ ,\end{aligned} \tag{6}$$

where $\overleftrightarrow{J}^{iT}$ is the transposed tensor of $\overleftrightarrow{J}^i$ and we have taken into account that all the quantities are real. The first term provides information on the amplitude of the field due to the spontaneous magnetization at site i and its symmetry around the c axis, while the remaining terms reveal the symmetry of site i in the plane perpendicular to the c axis. In the particular case that we shall consider the tensor $\overleftrightarrow{J}$ has a principal axis in the direction of $\vec{B}_{hf}$; as a consequence the last term in (6) will always be 0.

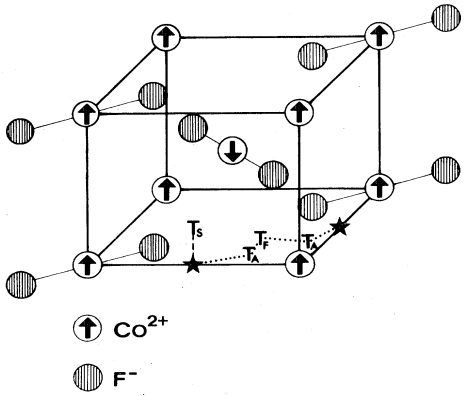

FIG. 5. Unit cell of CoF_2 and principal sites considered in Sec. IV for the localization of muons. Octahedral sites are indicated with an asterisk. T_A, O, and T_F sites are in the $(\hat{a},\hat{b})$ plane while T_S sites lie in the $(\hat{a},\hat{c})$ and $(\hat{b},\hat{c})$ planes. The symbols for the Co and F ions are not proportional to the respective ionic radii.

C. Description of the possible interstitial sites

We will examine now some possible sites of localization for the muon, selecting in particular those sites close to the fluorine anions characterized by a relatively large volume (essential for consideration involving zero-point energy of our light implanted particle). A simple calculation of the electrostatic potential has been carried out by assuming that the lattice is neither distorted nor polarized by the muon, and that the host lattice is composed of charged spheres. The sites that have been taken into consideration can be described with the help of Fig. 5.

1. Octahedral sites

O_a^α, O_a^β, O_s^α, and O_b^β are located at $(\pm0.5,0,0)$ and $(0,\pm0.5,0)$ for the α sublattice and at $(\pm0.5,0,\pm0.5)$, and $(0,\pm0.5,\pm0.5)$ for the β sublattice. These sites are characterized by six neighboring fluorine anions: two of them are in a polar position, at $(\lambda,\lambda,0)$ and $(1-\lambda,-\lambda,0)$,

where $\lambda=0.31$, at a distance of 1.77 Å from the center; the remaining four anions are equatorial and occupy the positions $(0.5+\lambda,0.5-\lambda,\pm0.5)$ and $(-0.5-\lambda,-0.5+\lambda,\pm0.5)$ at 2.42 Å from the center.

For both tensors $\overleftrightarrow{D}$ and $\overleftrightarrow{J}$, in these sites, there is a principal axis which coincides with the c axis: This is guaranteed by the mirror symmetry existing about the $z=0$ plane and it further ensures that $\vec{B}_{hf}$ is parallel to the c axis. The other two eigenvectors of the symmetric part of $\overleftrightarrow{J}$ lie in the $(\hat{a},\hat{b})$ plane; if we call $\Delta\varphi$ the angle that they make with the $\hat{a}+\hat{b}$ direction, the following relations can be derived from the crystal symmetries:

$$\begin{aligned}\Delta\varphi_a^\alpha &= -\Delta\varphi_b^\alpha ,\\ \Delta\varphi_a^\beta &= -\Delta\varphi_b^\beta ,\\ \Delta\varphi_b^\beta &= \tfrac{1}{2}\pi+\Delta\varphi_a^\alpha .\end{aligned} \tag{7}$$

The electrostatic potential in the O site is -2.5 V.

2. *Symmetric tetrahedral sites*

Every two neighboring O sites along the c axis share four fluorine anions. These anions define a tetrahedron, whose center will be called symmetric tetrahedral (T_S). There are eight T_S sites in the unit cell which are magnetically equivalent, being equidistant from both sublattices. Both $\overleftrightarrow{D}$ and $\overleftrightarrow{J}$ have in this case cylindrical symmetry, with the c axis as their principal axis. $\vec{B}_{hf}$ is therefore 0 also for $T<T_N$. The electrostatic potential in the T_S sites is -2.5 V, equal to that of the O sites, so that nearly equipotential channels exist in the lattice, parallel to the c axis, through (0,0.5,0) and (0.5,0,0) that contain alternated O and T_S sites.

3. *Asymmetric tetrahedral sites*

These sites, T_A, are surrounded by four fluorine anions. They can be identified as the center of the two tetrahedrons obtained by splitting each O site with a plane passing through the polar fluorines. There are eight T_A sites in the cell, two by two equivalent from the point of view of the tensors $\overleftrightarrow{D}$ and $\overleftrightarrow{J}$. Transformations among the T_A sites are obtained upon reflection in the planes normal to $\hat{a}+\hat{b}$ and $\hat{a}-\hat{b}$ as well as a 90° rotation around the c axis, followed by a translation of (0.5,0.5,0.5). The electrostatic potential in these sites is -1.2 V; both $\overleftrightarrow{D}$ and $\overleftrightarrow{J}$ have a principal axis coincident with the c axis. The symmetry of $\overleftrightarrow{J}$ in the $(\hat{a},\hat{b})$ plane is qualitatively the same as that of the O sites, which amounts to stating that the angles $\Delta\varphi$ obey (7).

4. *Fluorinelike tetrahedral sites*

These interstitial sites (T_F) have the symmetry of the fluorine anions. They can be almost exactly obtained by rotating the fluorine sites around the c axis by 90°: the resulting sites are contained in tetrahedrons of fluorine anions. $\vec{B}_{hf}$ is directed along $\hat{c}$, since the tensor $\overleftrightarrow{D}$ has this direction as a principal axis. The tensor $\overleftrightarrow{J}$ itself turns out to be symmetric in the T_F sites and it shares the same three axes of the susceptibility tensor, since they are principal axes for both $\overleftrightarrow{D}$ and $\overleftrightarrow{J}$. The electrostatic potential in the T_F sites is -0.78 V.

The ensemble of the sites described above defines a network of channels characterized by the sequence $\cdots$-O_a^α-T_A-T_F-T_A-O_b^α-T_A-T_F-T_A-O_a^β-$\cdots$. It seems that the O sites are the most stable, even if the values of the electrostatic potential are expected to change when the lattice polarization and deformation induced by the muon are included in the calculation.

D. Susceptibility tensor

The macroscopic susceptibility for CoF_2 is anisotropic both above and below T_N: $\chi_\perp$ is slightly larger than $\chi_\parallel$ up to $T\cong5T_N$. In addition, the cylindrical symmetry of $\overleftrightarrow{\chi}$ around the c axis is the result of the superposition of the susceptibilities χ_α and χ_β for the two sublattices α and β, which have different axes of symmetry ($\hat{a}+\hat{b}$ and $\hat{a}-\hat{b}$, respectively). By taking into account the ground-state properties of the Co^{2+} ions, Lines[9] provides the elements for evaluating χ_α and χ_β which are shown in Fig. 6, for

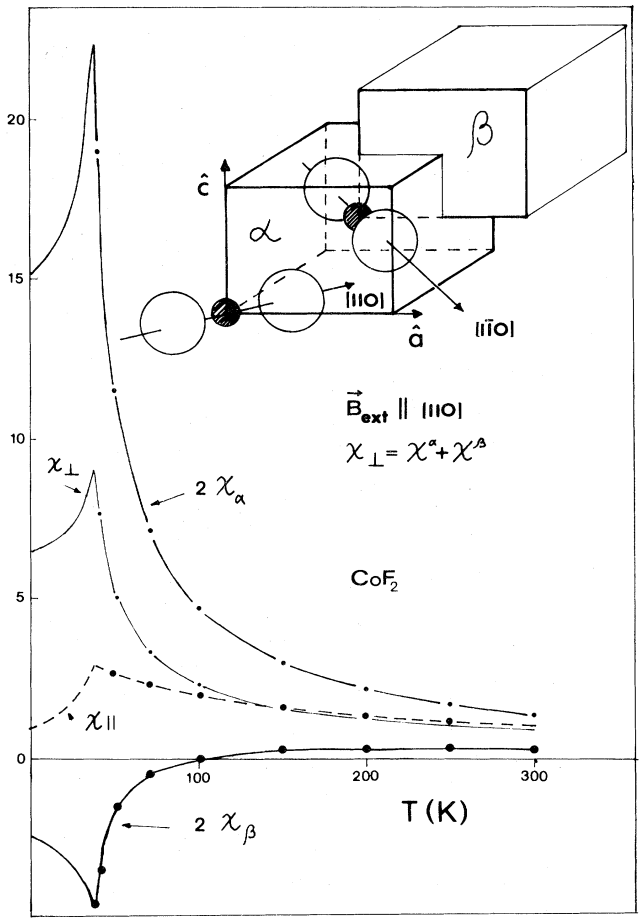

FIG. 6. Magnetic susceptibility for CoF_2 measured parallel and perpendicular to the c axis as a function of the temperature (from Ref. 9). The perpendicular susceptibility is isotropic in the $(\hat{a},\hat{b})$ plane, but the contributions from each sublattice are not. The susceptibilities for sublattices α and β are shown for an external field along the $(\hat{a},\hat{b})$ direction on a scale of $\times2$ for graphical purposes. χ_α and χ_β are calculated from Ref. 9.

TABLE I. Characteristics of the local magnetic fields at the sites considered in Sec. IV. R is the radius of the interstitial cavity, V is the electrostatic potential at each site for the undistorted lattice; D_α and D_β are the dipole field tensor contributions for each Co sublattice calculated for a Co magnetic moment of 2.64 Bohr magnetons—the listed values correspond to the *aa*, *ab*, *bb*, and *cc* elements of the tensors—all the others are 0; B_{hf} is the internal magnetic field in the presence of antiferromagnetic order: It is always parallel to the c axis for all the sites considered.

Site	R (Å)	V (V)	D_α (Å^{-3})				D_β (Å^{-3})				H_{hf} ($T=0$) (kG)
			aa	*ab*	*bb*	*cc*	*aa*	*ab*	*bb*	*cc*	
Octahedral O (0.5,0,0)	0.44	−2.545	0.292	0.0	−0.177	−0.115	−0.152	0.0	0.159	−0.006	−2.65
Symmetric tetrahedral T_S (0.5,0,0.25)	0.62	−2.545	0.222	0.0	−0.164	−0.058	−0.164	0.0	0.222	−0.058	0.0
Asymmetric tetrahedral T_A (0.65,0.84,0)	0.59	−1.2	0.383	−0.104	−0.211	−0.173	−0.123	−0.031	0.123	0.0	−4.3
Fluorinelike tetrahedral T_F (0.69,0,31,0)	0.52	−0.78	0.058	−0.140	0.058	−0.117	−0.093	−0.12	−0.093	0.186	−7.42
Center base C_B (0.5,0,5,0)	0.0	0.02	0.036	0.0	0.036	−0.072	−0.486	0.0	−0.486	0.972	−25.6

the case of an external field parallel to the $\hat{a}+\hat{b}$ direction. Such properties of CoF_2, and in particular the opposite sign of χ_α and χ_β below $T \cong 3T_N$, are quite important in determining the magnetic properties of the crystal (weak ferromagnetism, staggered induced magnetization,[10,11] etc.), and are very interesting for the present study of muon localization in view of the resulting symmetry that the tensor $\overleftrightarrow{J}$ takes.

E. Local magnetic fields

For each site of localization i, the knowledge of the tensors $\overleftrightarrow{D}^i$, $\overleftrightarrow{J}^i$, and $\overleftrightarrow{\chi}$ enables the calculation of the local field $\vec{B}^i_\mu$. This is achieved by making use of the expression (3), for the paramagnetic phase (where splittings and/or shifts of the muon precession frequencies are relevant), or of expression (4) in the ordered phase, when the value of $|\vec{B}^i_{hf}(T=0)|$ itself is required. If we assume that the magnetic field at each site i is determined by point dipoles localized only on the metal ions of the undistorted lattice, the tensor $\overleftrightarrow{D}$ will simply be given by

$$(\overleftrightarrow{D}^i_\alpha)_{jk} = \sum_{l=1}^{N} \frac{3(\vec{r}_{i1}\cdot\vec{x}_j)(\vec{r}_{i1}\cdot\vec{x}_k) - \delta_{jk} r_{i1}^2}{r_{i1}^5}, \tag{8}$$

where $\vec{r}_{i1}$ joins the site i with the lth cation of sublattice α (the identical treatment can be followed for $\overleftrightarrow{D}_\beta$).

Table I reports the values of the calculated components of the dipole field tensor in the paramagnetic phase and the modulus of $\vec{B}_{hf}$ at $T=0$ K. The choice of the appropriate g factor for the ground state at low temperatures is not trivial for Co ions. Lines[9] has discussed the problem thoroughly and the assumed value for CoF_2 is then $g_{||}=2.64$; the values in Table I are calculated using this and the other components of the g tensor from the same source.

For all sites i in the paramagnetic phase one expects a single line when $\vec{B}_0$ is parallel to $\hat{c}$. A splitting takes place when $\vec{B}_0$ is perpendicular to $\hat{c}$ (except for T_S) with symmetries in the $(\hat{a},\hat{b})$ plane which depend on the site. Figure 7 summarizes the angular dependence predicted for the various centers at 40 K. Quantitative changes take place as a function of temperature since both χ_α and χ_β are strongly temperature dependent.

By comparing expressions (3) and (4), it is evident that the same angular dependence of the shifts and the splittings is expected in the antiferromagnetic region as well. It must be pointed out, however, that in this case an external field splits the muon frequency into two components, one for each sublattice (an exception is the case $\vec{B}_0 \perp \vec{B}_{hf}$, when the resulting field on each sublattice is the same in absolute value). The precession frequencies of each sublattice will reflect the pattern of the paramagnetic phase if, as generally is the case, the ordered phase is characterized by a domain structure.

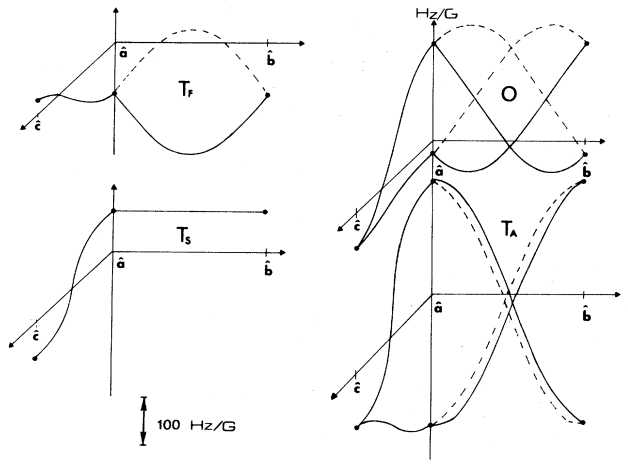

FIG. 7. Calculated angular dependence of the shift and splittings of the muon precession signal in CoF_2 at 40 K for the various sites of localization considered in Sec. IV. In the $(\hat{a},\hat{c})$ plane no distinction is, in principle, possible for the two sublattices, while in the $(\hat{a},\hat{b})$ plane one sublattice follows the dashed line while the other follows the solid line. Such distinction may be relevant, however, only if an experiment is carried out in the ordered phase on a single-domain crystal.

V. DISCUSSION OF THE RESULTS

A. Localization in CoF_2

Figure 8 shows a summary of the data on the frequency shifts and splittings in the same format as Fig. 7. The results from the antiferromagnetic phase have been included after appropriate scaling of the origin: The temperature of the two sets of measurments—below and above T_N—had been chosen in the experiments in order to have nearly the same value of the susceptibility in both cases.

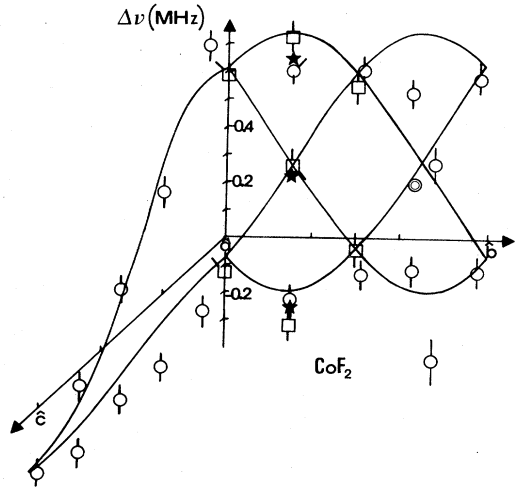

FIG. 8. Summary of the experimental results and comparison with the calculations for the octahedral site. The c- to a-axis portion is part of Fig. 2; the a- to b-axis portion contains the results obtained with the wire-chamber spectrometer (asterisks), those obtained at low temperatures as shown in Fig. 4 (squares), and those obtained with the scintillator spectrometer at 40 K (circles): For these data the concentric circles represent a signal whose presence can only be conjectured from the Fourier spectrum, but hardly fitted at all due to its proximity to the background "cryostat" signal and to the relatively small amplitude. All data are for an external field of 3 kG.

The comparison between Figs. 7 and 8 demonstrates that the sites occupied by the muons are the O sites. This conclusion relies heavily on the angular dependence of the frequencies in the $(\hat{a},\hat{b})$ plane. Close inspection of the behavior in the $(\hat{a},\hat{c})$ plane, however, shows that the models can be discriminated already on the basis of this subset of data. The splitting on approaching the a axis and the asymmetry of the shifts of the two sublattices along this direction, with respect to the c-axis value, correspond to what is expected for the O sites only.

The magnitude of the shifts, which has a maximum of 67 ± 6 G between extreme components at 22.5° from the a axis in the $(\hat{a},\hat{b})$ plane, compares well with the first-principles estimates of 69 G. This fact strongly suggests that the local field at the muon is almost exclusively the distant dipole field of the Co ion moments.

The observed behavior also allows us to evaluate the phase angle $\Delta\varphi$, defined in expression (7), which depends on the actual symmetry of the two sublattices transverse susceptibility, $\chi_{\perp}^{\alpha}$ and $\chi_{\perp}^{\beta}$: The experimental value is then $20°\pm2°$, consistent with that evaluated using the data from Ref. 9.

The measured value of the local field sensed by the muons in the ordered phase, $\vec{B}_{hf}(T=0)$, which is of 2288 G, agrees satisfactorily with the 2650 G calculated for the magnetic field of a rigid lattice of point dipoles: the 16% discrepancy which remains will be discussed in the following section.

B. Localization in MnF_2

Previous measurements on this material[5] indicate that only 35% of the detected muons contributed to the precession signal above T_N, while no evidence of a precession was then found below T_N. The discussion of Sec. IV on the candidate sites of occupancy for a light positive impurity applies equally well to MnF_2: The available sites are the octahedral site and the three kinds of tetrahedral sites shown in Fig. 6. By analogy to the case of CoF_2, the octahedral symmetry is expected, as the structural differences between the two crystals are very small.

A difference relative to the cobalt crystal, which is of relevance for the experimental results, is that the susceptibilities of the single sublattices are scalar above T_N and they split into two components, $\chi_{||}$ and $\chi_{\perp}$, below T_N. As a consequence the properties of symmetry revealed by paramagnetic shift measurements depend only on the nature of the tensor $\overleftrightarrow{D}$, to which $\vec{J}$ is simply proportional.

Figure 9 shows the results of a set of measurments performed at 71 K, where the magnetic field was applied along various directions in the $(\hat{a},\hat{c})$ plane. The fitting procedures that give the frequencies reported on the plot are the same as those described for CoF_2 in relation to Fig. 2. The same pattern appears here; the value for the splitting along the a axis for MnF_2 is 500 KHz while the calculated values are 480 and 220 KHz for the T_A and O sites, respectively. The other sites considered in Sec. IV are ruled out because they do not predict any splitting along the a axis.

In the remainder of this section we describe the difficulties encountered in the study of the localization of

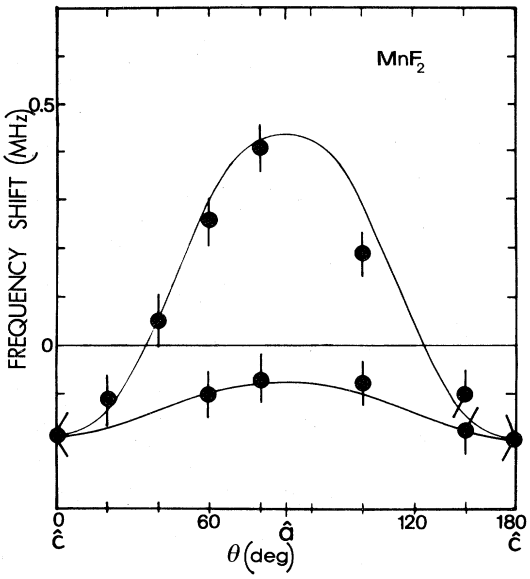

FIG. 9. Angular dependence of the muon precession signal in MnF_2 at 71 K in 3 kG. The solid line is a guide to the eye. The calculated curves of Sec. IV indicate that only O and T_A sites are compatible with the experiments.

muons in MnF_2 Such difficulties prevented a more certain choice of the site between O and T_A sites.

As mentioned earlier, and in contrast to CoF_2, the μSR signals in the paramagnetic phase of MnF represent only 35% of the total implanted muons. In addition, for $T<T_N$, a further drastic loss in signal amplitude takes place. The maximum polarization detected in this case corresponds to less than 5% of all implanted muons. Under these conditions it is both difficult and time consuming to obtain good signal-to-noise ratios. Only three temperatures have therefore been considered: 15, 40, and 62 K which correspond approximately to $0.25T_N$, $0.6T_N$, and $0.9T_N$, respectively. In longitudinal geometry with zero-applied field and the c axis perpendicular to the beam polarization no signal was detected at the intermediate temperature. At 15 K two frequencies were observed with a signal-to-noise ratio of 2 in. amplitude, at 67 and 169 MHz, while at 62 K only one signal was detected at 36 MHz.

The predictions from the model calculations for the O and T_A sites are 61 and 96 MHz, respectively, and a comparison with available data will certainly suffer from the poor degree of confidence associated with the low signal-to-noise ratios.

VI. CONCLUSIONS

The determination of the muon localization in CoF_2 as an octahedral site occupancy is confirmed beyond any doubt by the different experiments performed over a large range of temperatures (13–40 K). The μSR method provides, in this case, a direct means of studying the components of the susceptibility tensor for each sublattice. This is of particular relevance for anisotropic systems, such as CoF_2. The analysis of the amplitude ratios of the signals detected in the ordered phase confirms the ex-

istence of magnetic domains in the crystal, equally distributed between the two possible orientations.

There remains a small discrepancy between the hyperfine field measured below T_N and the present estimates. In principle, this could be due to either of the approximations made in Sec. IV: First of all, we assumed the electron spin to be localized on the Co^{2+} ions only while there could exist a partial delocalization on the F^- ions (as it is known from NMR measurements on the ^{19}F nuclei); second of all, the lattice was considered undistorted by the presence of the muon, whereas lattice relaxation is to be expected. The first correction seems to be negligible as it would inevitably reduce the agreement between the predicted and the measured value of $\Delta\varphi$. This allows us to infer that the muon does not participate in a real chemical bond within the CoF_2 lattice; a similar behavior has been predicted for transition-metal oxides[12] and has been observed in some rare-earth orthoferrites.[13]

Lattice relaxation around the muon remains the more likely cause of the 16% difference between the hyperfine field measured and calculated values. For the octahedral site we have estimated that such a difference corresponds to a displacement of the neighboring Co^{2+} ions by a few percent of their distance from the site.

The signal amplitudes deserve a short discussion; the fraction of muons which is not observed even at 300 K (30% for CoF_2 and 64% for MnF_2) could be accounted for by the formation of muonium, whose observation in the present experiments would be precluded by strong magnetic perturbations. In similar crystals, where the perturbation is limited to the nuclear dipole moments, muonium has been actually detected,[14] even if in MnF_2 the absence of this state is claimed from longitudinal-field experiments.[15].

The sudden reduction of amplitude across the Néel point is of relevance to the muon localization. It cannot be explained by invoking another stopping site for the implanted particles as it should give rise to an independent signal at a different frequency in the ordered phase, which has not been observed. In addition, all the detected muons in the paramagnetic phase display the same symmetry in the splittings, which is characteristic of the O sites.

For this reason a different explanation is more plausible: A portion of the implanted particles can stop in the vicinity of a defect or of an impurity. The latter can actually catalyze the localization, which might take place in the same interstitial site as in the absence of defects. The magnitude of the local field sensed by the muon can, however, change over a range of values. This has different effects depending on the temperature regions: In the paramagnetic phase a hypothetical 20% spread of the local field would barely be noticeable in the shift pattern of the Larmor frequency while, below T_N, the same spread would cause a very fast decay of the signal up to an eventual disappearance from the experimental histogram.

In MnF_2 the available data clearly indicate that the T_F and T_S sites cannot be occupied by the muons, while discrimination between the two neighboring sites O and T_A is made difficult essentially by the weakness of the signal. In this connection, and in contrast to the CoF_2 crystal, the uniqueness of the localization site in MnF_2 may not be valid in the broad range of temperature between $T=0$ K and the paramagnetic phase $T>70$ K. The coexistence of both sites as well as possible transitions between O and T_A that are thermally activated are not only plausible processes in this temperature range, but they could be responsible for the absence of a unique and coherent local field in the ordered phase. It must be noted, however, that the situation in the ordered phase can be justified with the same mechanism that was invoked for the partial loss of signal intensity for CoF_2. Interestingly, the phenomenon of partial loss in signal intensity in the ordered phase seems to be rather general, as it has been observed, for instance, also in the NMR studies of several antiferromagnetic crystals.[16]

ACKNOWLEDGEMENTS

The authors appreciate the assistance of Dr. T. Niinikoski and Mr. G. Coubra of the Polarized Target Group at CERN for the low-temperature equipment, the constant attention of the CERN Synchrocyclotron Machine (MSC) group to the beam-related problems of the experiments, the collaboration of the personnel of the x-ray division of the National Research Council (CNR) Maspec Laboratory for the single-crystal orientations, the valuable comments and suggestions of Professor L. Reatto, and the assistance of Dr. A. Jeavons and M. R. Magnanini during the initial operation of the wire-chamber spectrometer. This work was supported by the Consiglio Nazionale delle Ricerche, Rome, and by the Experimental Physics Division of CERN, Geneva. Part of the experimental equipment was supported by Instituto Nazionale di Fisica Nucleare (INFN) Milan. One of us (R.D.R.) gratefully acknowledges partial support for the present work granted by Rutherford Appleton Laboratory (Oxfordshire).

[1]P. Heller, in *Local Properties at Phase Transitions,* edited by K. A. Mueller and A. Rigamonti (North-Holland, Amsterdam, 1976), p. 447.

[2]V. Jaccarino, Phys. Rev. Lett. **2**, 163 (1959).

[3]R. A. Cowley, W. J. L. Buyers, P. Martel, and R. W. H. Stevenson, J. Phys. C **6**, 2997 (1973).

[4]S. J. Allen and H. J. Guggenheim, Phys. Rev. B **4**, 937 (1971).

[5]R. De Renzi, R. Tedeschi, G. Guidi, C. Bucci, and S. F. J. Cox, Solid State Commun. **43**, 683 (1982).

[6]R. De Renzi, R. Tedeschi, G. Guidi, C. Bucci, and S. F. J. Cox, in *Europhysics Conference Abstracts,* edited by V. Heine (European Physical Society, Petit Lancy, Switzerland, 1982), p. 407.

[7]CERN-μSR Collaboration, Report No. 1 1980 (unpublished).

[8]R. Tedeschi, P. Podini, R. De Renzi, A. P. Jeavons, R. Magnanini, and L. O. Norlin, Nucl. Instrum. Methods **214**, 509 (1983).

[9]M. E. Lines, Phys. Rev. **137**, A982 (1965).

[10]A. N. Bazhan and Ch. Bazan, Zh. Eksp. Teor. Fiz. **69** 1768 (1975). [Sov. Phys.—JETP **42** 898 (1976)].

[11]N. Giordano and W. P. Wolf, Phys. Rev. B **21**, 2008 (1980).
[12]D. Ellis and B. Lindgren, Hyperfine Interactions **17**, 279 (1984).
[13]E. Holzschuh, W. Kuendig, and A. B. Denison, Hyperfine Interations **17**, 345 (1984)..
[14]B. D. Patterson (private communication).
[15]Y. J. Uemura (private communication).
[16]C. Bucci and G. Guidi, in *Local Properties at Phase Transitions,* edited by K. A. Mueller and A. Rigamonti (North-Holland, Amsterdam, 1976), p. 624.